# Rotational band structure in $^{32}$Mg

H. L. Crawford,[1,2,*] P. Fallon,[1] A. O. Macchiavelli,[1] A. Poves,[3] V. M. Bader,[4,5] D. Bazin,[4] M. Bowry,[4] C. M. Campbell,[1]
M. P. Carpenter,[6] R. M. Clark,[1] M. Cromaz,[1] A. Gade,[4,5] E. Ideguchi,[7] H. Iwasaki,[4,5] C. Langer,[4] I. Y. Lee,[1] C. Loelius,[4,5]
E. Lunderberg,[4,5] C. Morse,[4,5] A. L. Richard,[2] J. Rissanen,[1] D. Smalley,[4] S. R. Stroberg,[4,5] D. Weisshaar,[4] K. Whitmore,[4,5]
A. Wiens,[1] S. J. Williams,[4] K. Wimmer,[8] and T. Yamamato[7]

[1]*Nuclear Science Division, Lawrence Berkeley National Laboratory, Berkeley, California 94720, USA*
[2]*Institute for Nuclear and Particle Physics and Department of Physics and Astronomy, Ohio University, Athens, Ohio 45701, USA*
[3]*Departamento de Fisica Teorica and IFT-UAM/CSIC, Universidad Autonoma de Madrid, E-28049 Madrid, Spain*
[4]*National Superconducting Cyclotron Laboratory, Michigan State University, East Lansing, Michigan 48824, USA*
[5]*Department of Physics and Astronomy, Michigan State University, East Lansing, Michigan 48824, USA*
[6]*Physics Division, Argonne National Laboratory, Argonne, Illinois 60439, USA*
[7]*RCNP, Osaka University, Mihogakoa, Ibaraki, Osaka 567-0047, Japan*
[8]*Department of Physics, The University of Tokyo, Bunkyo-ku, Tokyo 113-0033, Japan*
(Received 7 January 2016; published 23 March 2016)

There is significant evidence supporting the existence of deformed ground states within the neutron-rich $N \approx 20$ neon, sodium, and magnesium isotopes that make up what is commonly called the "island of inversion." However, the rotational band structures, which are a characteristic fingerprint of a rigid nonspherical shape, have yet to be observed. In this work, we report on a measurement and analysis of the yrast (lowest lying) rotational band in $^{32}$Mg up to spin $I = 6^+$ produced in a two-step projectile fragmentation reaction and observed using the state-of-the-art $\gamma$-ray tracking detector array, GRETINA ($\gamma$-ray energy tracking in-beam nuclear array). Large-scale shell-model calculations using the SDPF-U-MIX effective interaction show excellent agreement with the new data. Moreover, a theoretical analysis of the spectrum of rotational states as a function of the pairing gap, together with cranked-shell-model calculations, provides intriguing evidence for a reduction in pairing correlations with increased angular momentum, also in line with the shell-model results.

Exotic combinations of neutrons ($N$) and protons ($Z$) found far from beta stability can significantly affect nuclear structure and properties. The spin-isospin components of the nucleon-nucleon effective interaction [1] can alter the spacing and even the ordering of single-particle states, giving rise to changes in shell structure and to new regions of deformation and collectivity. The region of neutron-rich nuclei centered on $^{32}_{12}$Mg is archetypal of this phenomenon of shell evolution and has been the subject of intense experimental and theoretical work [2–7]. Here, the $N = 20$ spherical shell gap, while known to be large near stability, is significantly reduced. As a result, open-shell configurations are energetically favored whereby neutron pairs promoted across the $N = 20$ gap (from $sd$ to $pf$ orbitals) take advantage of the strong quadrupole-quadrupole component of the effective force, leading to highly correlated deformed ground states rather than the *a priori* expected spherical states. These states are characterized by $n$-particle-$n$-hole ($n$p-$n$h) configurations, where $n$ is predominantly 2 and 4. Early mean-field calculations [3] were the first to suggest the occurrence of deformation in this region to explain the excess of binding in the $^{31}$Na ground state, but *ad hoc* rotational correlations were required to obtain the deformed minimum.

There is a significant body of experimental evidence supporting the existence of deformed ground states within the neutron-rich $N \approx 20$ neon, sodium, and magnesium isotopes that make up what is commonly called the "island of inversion." Shape coexistence has also been clearly identified at the center of this region, with a low-lying $0_2^+$ state observed in $^{32}$Mg [8]. However, rotational band structures, which are a characteristic fingerprint of nonspherical shapes, have not yet been firmly established. Without such data, our knowledge of the microscopic dynamics leading to the development and evolution of deformation in this region remains incomplete.

Here, we report on a measurement and analysis of the yrast (lowest lying) rotational band in $^{32}$Mg up to spin $I = 6^+$, produced in a two-step projectile fragmentation reaction and observed using the state-of-the-art gamma ray tracking detector array, GRETINA ($\gamma$-ray energy tracking in-beam nuclear array) [9]. We chose a secondary fragmentation reaction that maximizes the number of nucleons removed from the projectile with the aim of populating states with higher total angular momentum $I$. It is expected that the angular momentum imparted to a nucleus in such a reaction is related to the mass difference between the projectile and the final fragment nucleus [10]. However, the removal of many nucleons also leads to a much-reduced production cross section for the nucleus of interest, relative to other channels. In this experiment we used a radioactive beam of $^{46}$Ar to produce $^{32}$Mg, corresponding to the removal of 14 nucleons (8 neutrons and 6 protons), in order to simultaneously optimize the production cross section and reach higher spin states in $^{32}$Mg.

The $^{46}$Ar secondary beam was produced at the National Superconducting Cyclotron Laboratory (NSCL) at Michigan State University, following fragmentation of an intense 140 MeV/u $^{48}$Ca primary beam on a 846 mg/cm$^2$ $^9$Be target
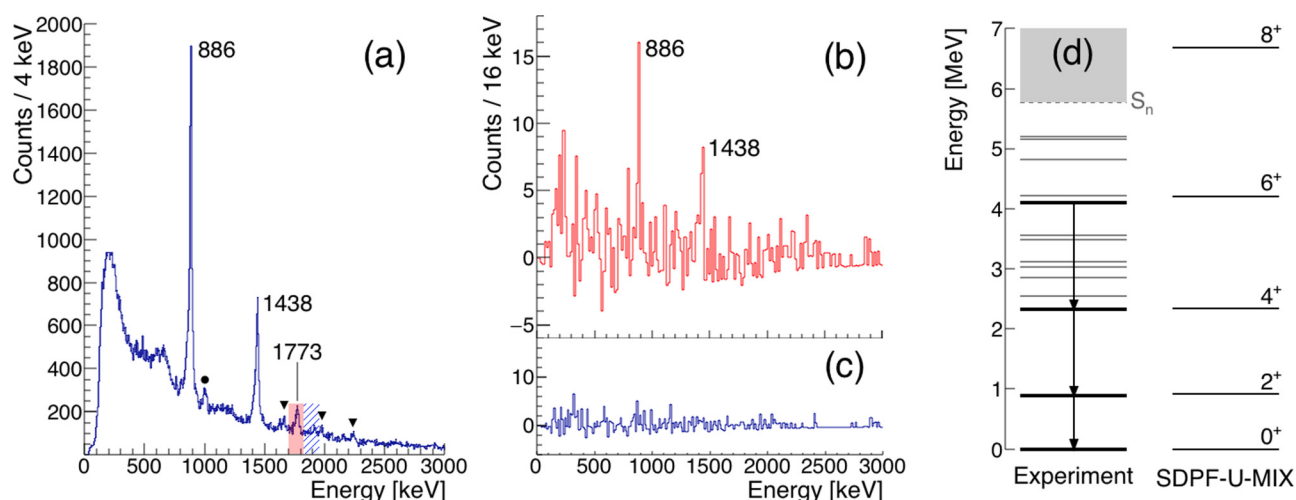
---

FIG. 1. (a) Prompt $\gamma$-ray spectrum detected with GRETINA in coincidence with $^{32}$Mg heavy recoils following secondary fragmentation of a $^{46}$Ar beam at the target position of the S800; other previously observed transitions are marked by inverted triangles (see text). (b) Spectrum of $\gamma$ rays in coincidence with the 1773 keV transition (red shaded region) obtained from a background-subtracted $\gamma$-$\gamma$ correlation matrix [see Eq. (3) in Ref. [13]]. (c) Similar to panel (b) but now in coincidence with an energy region ("background") immediately above the proposed 1773 keV $\gamma$ ray (blue hashed region). The 886 and 1438 keV transitions are visible in the 1773 keV gated spectrum (panel b), but not in the "background" gated spectrum [panel (c)]. (d) Experimental excitation energies for the known levels in $^{32}$Mg [8,14,15], including the ground-state rotational band states observed in the present work (bolded lines) and shell-model excitation energies for the lowest-lying (yrast) rotational states.

located at the entrance of the A1900 fragment separator [11]. $^{46}$Ar was separated from other primary fragmentation products through the A1900 based on magnetic rigidity and energy loss through an Al wedge degrader and delivered to the S3 experimental area with a momentum acceptance $\Delta p/p$ of 1%, an incoming energy of 102 MeV/u, and better than 95% beam purity. $^{32}$Mg ions along with a cocktail of other products were then produced by fragmenting the $^{46}$Ar on a 267 mg/cm$^2$ thick $^9$Be target located at the target position of the S800 spectrograph [12]. The S800 was used to unambiguously identify final products on an ion-by-ion basis through their time of flight, energy loss, and total energy as measured in the detectors of its focal plane, allowing detection and identification of $^{32}$Mg produced with a yield of approximately 0.14/10$^6$ incoming $^{46}$Ar particles. The measured focal-plane positions, together with the optics model for the spectrograph also provide information on the ion trajectory following the reaction.

The $\gamma$ rays emitted from excited nuclear states were detected by seven GRETINA detector modules surrounding the S800 target. For this measurement, the modules were placed at 90° to the beam direction to minimize the interaction of light ions and neutrons produced in the reaction, which are forward (0°) focused. The incoming $^{46}$Ar beam on target was limited to $4 \times 10^6$ pps, and the maximum rate in a single GRETINA crystal was then ~15 kHz.

Each GRETINA module consists of four closely packed high-purity germanium crystals (28 in total), where each crystal is itself electrically segmented into 36 elements. The high degree of segmentation allows the positions and energies of individual $\gamma$-ray interaction points to be measured and tracked. The $\gamma$-ray interaction position information from GRETINA and the particle trajectory information from the S800 were used to provide an accurate event-by-event Doppler

correction for the observed $\gamma$ rays, which are emitted in flight from nuclei traveling at about 40% the speed of light. An overall energy resolution of ~2% was achieved after Doppler correction. $\gamma$-ray yields were determined based on a fit to data with a complete GEANT4 simulation of the GRETINA response, which reproduces source efficiencies to within 1%.

The left panel of Fig. 1 shows the spectrum of $\gamma$ rays observed in GRETINA and emitted from excited states in $^{32}$Mg. Three strong transitions are seen at 886(4), 1438(4), and 1773(4) keV with relative (total) intensities of 100%, 52%, and 12%, respectively. The first two correspond to the known $\gamma$ rays at 885 and 1436 keV, which have been assigned to the $2_1^+ \to 0_1^+$ and $4_1^+ \to 2_1^+$ decays based on angular correlations [14]. The transition at 1773 keV is new. Previous works have clearly established the collective character of the 885 keV transition [16–19], and that the 885 and 1436 keV transitions form a $4 \to 2 \to 0$ cascade [14]. The $\gamma$-$\gamma$ coincidence spectra [Figs. 1(b) and 1(c)] place the 1773 keV $\gamma$ ray in coincidence with the $2_1^+$ and $4_1^+$ states and within this cascade. We assign it to be the $6_1^+ \to 4_1^+$ transition and the third member of the ground state (yrast) rotational band lying at an excitation energy of 4097(7) keV. We would also like to point out that the intensities of the $2^+$, $4^+$, and $6^+$ transitions observed here are consistent with a statistical population as described in Ref. [20]. Moreover, the fact that the new transition was not observed in previous direct reactions, $\beta$-decay studies, or scattering measurements [14,15,21,22] is consistent with the selective spin population and statistics in these previous experiments.

The other transitions observed in Fig. 1(a) above 1.6 MeV, and marked with inverted triangles; namely, at 1660, 1975, and 2238 keV, correspond to $\gamma$ rays identified in previous works and assigned as depopulating low-spin ($I < 4$) states [14,15].

TABLE I. Yrast states in $^{32}$Mg up to $I = 8$. Experimental level information (left side of the table) was taken from this present work. Shell-model calculations, on the right side of the table, use the SDPF-U-MIX effective interaction as discussed in the text and include the calculated intrinsic quadrupole moment $Q_0$ and $B(E2 : 2_1^+ \rightarrow 0_1^+)$ transition rates.

| | Experiment | | Shell model (SDPF-U-Mix) | | | |
| | $E$ | $I_\gamma$ | $E$ | $Q_0$ | $B(E2 \downarrow)$ | |
| $I^\pi$ | [keV] | (rel.) | [keV] | [$e\,\mathrm{fm}^2$] | [$e^2\,\mathrm{fm}^4$] | 2p-2h/4p-4h |
|---|---|---|---|---|---|---|
| $0^+$ | 0 | | 0 | | | 53/37 |
| $2^+$ | 886(4) | 1.00 | 920 | 67 | 90 | 43/54 |
| $4^+$ | 2324(6) | 0.52 | 2340 | 68 | 137 | 31/68 |
| $6^+$ | 4097(7) | 0.12 | 4210 | 68 | 153 | 31/68 |
| $8^+$ | | | 6680 | 71 | 113 | 10/90 |

The transition at 1 MeV and marked with a circle is previously unobserved. However, with the low statistics we cannot place it in the level scheme for $^{32}$Mg.

The $^{32}$Mg rotational-band energies observed in this work are summarized in Fig. 1(d) and Table I together with the results of a large-scale shell-model calculation shown up to spin $I^\pi = 8^+$. The agreement is excellent up to and including the assigned $6^+$ state. The calculations were carried out with the ANTOINE code using the SDPF-U-MIX effective two-body interaction, which includes the $sd$-$pf$ valence space and allows mixing between different $n$p-$n$h configurations (details are given in Ref. [23]). The results of the shell-model calculation presented in Table I indicate a change in the structure of the rotational band with increasing spin, from a highly mixed $0^+$ and $2^+$ state to a predominantly 4p-4h $8^+$ state. The complexity of the wave functions, especially those of the low-spin, i.e., $0^+$, states is particularly worth noting. $^{32}$Mg is a unique system in which shell-model-described deformed (2p-2h), superdeformed (4p-4h), and spherical (0p-0h) bands exist at similar excitation energies and mix substantially. Remarkably though, even with the complex and evolving microscopic structure of the yrast band, the calculations predict an intrinsic quadrupole moment, $Q_0$, that remains unchanged with increasing spin, indicating a near-constant value for the quadrupole deformation, $\epsilon_2 \approx 0.4$, throughout the band, corresponding to an ellipsoidal major/minor axis ratio of ~1.55.

A plot of spin ($I_x$) versus angular frequency ($\hbar\omega_x$) for the $^{32}$Mg rotational band is shown in Fig. 2 for both the experimental data and shell-model calculation. The angular frequency is given by

$$\hbar\omega_x(I) \equiv \frac{\partial E(I)}{\partial I_x(I)} \approx \frac{E(I+1) - E(I-1)}{2} = \frac{E_\gamma}{2}, \quad (1)$$

where $E = \frac{\hbar^2}{2\mathcal{J}} I(I+1)$, and $\frac{\mathcal{J}}{\hbar^2} = I/\hbar\omega$ is the moment of inertia. The red dashed line indicates the rigid-rotor limit

$$\frac{\mathcal{J}_{\mathrm{rig}}}{\hbar^2} = \frac{A^{5/3}}{72}\left(1 + \frac{1}{3}\epsilon_2 + \frac{11}{18}\epsilon_2^2 + \cdots\right) \quad (2)$$

for $^{32}$Mg calculated by using a deformation $\epsilon_2 = 0.4$. The data and shell-model calculation show a clear increase in $\mathcal{J}$, going
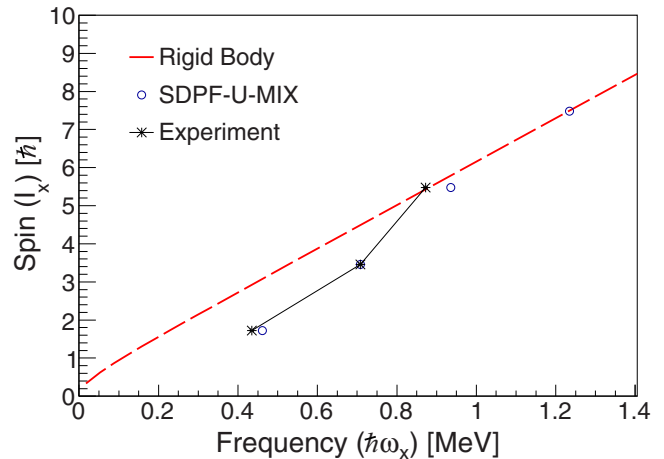


FIG. 2. Spin ($I_x$) versus angular frequency ($\hbar\omega_x$) for the ground-state band. Experimental points are plotted as asterisks (connected by the solid black line) while the results of large-scale shell-model calculations using the SDPF-U-MIX effective interaction are shown in blue open circles. The red dashed line shows the rigid-rotor limit for this nucleus assuming an axially symmetric prolate shape with a deformation $\epsilon_2 = 0.4$.

from roughly one half of the rigid-body value for the $2^+$ state and reaching the rigid-body value at spin $6^+$. A changing moment of inertia reflects a change in the structure [24]; for example, deformation, pairing ("superfluid") correlations, or the alignment of specific valence nucleon configurations with the axis of rotation (often discussed in terms of a band crossing).

We have seen that, within the framework of the shell-model calculation (Table I), the increase in $\mathcal{J}$ is correlated with an increasing fraction of the 4p-4h component in the shell-model wave function, but not a change deformation. It is therefore possible that the change in $n$p-$n$h composition (i.e., the mixing within the shell model) could be understood in terms of a mean-field description that naturally captures the $n$p-$n$h mixing in the intrinsic states, and the evolution with angular momentum by way of quasiparticle alignments. Furthermore, the moment of inertia for the $2^+$ state is appreciably smaller than the rigid value and suggests the presence of pairing correlations. An estimate of $\mathcal{J}/\mathcal{J}_{\mathrm{rig}}$ as a function of the ratio $\epsilon_2\hbar\omega_\circ/2\Delta$ ($\hbar\omega_\circ = 41$ MeV $\times A^{-1/3}$) that measures the competition between single-particle energies ($\epsilon_2\hbar\omega_\circ$) and pairing correlations ($2\Delta$) can be obtained from Ref. [24]:

$$\frac{\mathcal{J}}{\mathcal{J}_{\mathrm{rig}}} \approx \left(\frac{1}{1 + (2\Delta/\epsilon_2\hbar\omega_0)^2}\right)^{3/2}, \quad (3)$$

and yields a value of $\Delta \approx 2$ MeV for the $^{32}$Mg ground-state pairing gap, in line with that expected from systematics ($\Delta = 12$ MeV/$A^{1/2}$) and ground-state mass differences. Moreover, the fact the band reaches the rigid-rotor limit (for $\epsilon_2 = 0.4$) at higher spins could indicate that the changing $\mathcal{J}$ is due to a reduction of $\Delta(I)$ by about a factor of two. While the properties of the rotational band are well described
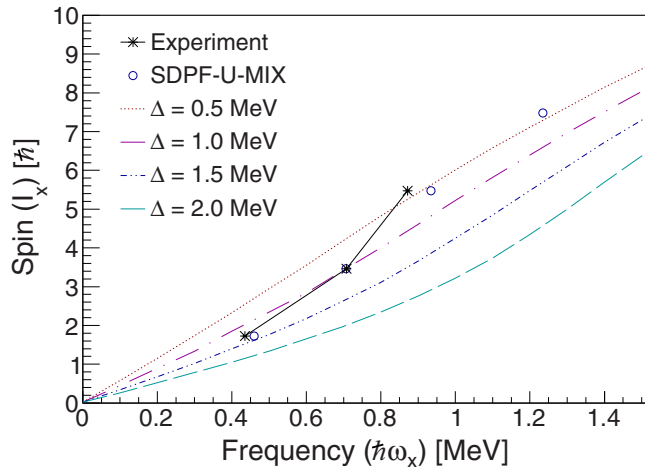
FIG. 3. Spin ($I_x$) vs angular frequency ($\hbar\omega_x$) for the ground-state band; experimental points are plotted as asterisks and connected by the solid black line, while the open blue circles are the results of shell-model calculations. The colored curves correspond to the results of CSM calculations performed with different values for the pairing gap, $\Delta_{n,p}$ ranging from 2.0 to 0.5 MeV.

by the large-scale shell-model calculation as discussed, the interplay between ingredients such as pairing and particle-(quasi)particle alignments is not so clear.

To provide further insight into the nature of the structural change(s) within the $^{32}$Mg band, in a mean-field description we carried out a cranked-shell-model (CSM) [25,26] calculation using the tilted-axis cranking (TAC) code [27]. The CSM describes the motion of independent-(quasi)particles in a rotating nucleus with a static deformed shape and pair field (associated with a pairing gap $\Delta$) and provides a method to analyze the effects of deformation, pairing, and rotational alignments. The results are shown in Fig. 3, plotted as a function of the spin and frequency similar to Fig. 2, for constant deformation $\epsilon_2 = 0.4$ and with fixed (and equal) neutron and proton pairing gaps ($\Delta_{n,p}$). The set of colored curves map out the total (proton + neutron) spin as a function of $\hbar\omega$ for differing pair gaps ranging from 2.0 to 0.5 MeV. The experimental data and shell-model calculation results are also included in the plot. The $\Delta = 1.5$ MeV curve passes through the $I = 2^+$ data point, as may have been anticipated, but does not follow the subsequent sharp up-bend in $I$ vs $\hbar\omega$. Indeed all the constant pairing curves (at $\epsilon_2 = 0.4$) exhibit a far more gradual change in $I$ vs $\hbar\omega$ over the relevant frequency range and none reproduce the data. We note, the curves associated with an increasingly reduced pair gap "track" the data, with the $\Delta = 0.5$ MeV curve coming close to the $6^+$ value, in line with the analysis of $\mathcal{J}/\mathcal{J}_{\rm rig}$ as a function of $\epsilon_2\hbar\omega_\circ/2\Delta$ discussed above. The CSM results lead to the important finding that the observed increase in $\mathcal{J}$ is inconsistent with a simultaneously constant pair gap and constant deformation scenario and suggests that a reduction in pairing with increasing spin is (at least) part of the underlying physics describing the $^{32}$Mg band. This result is consistent with that of the shell model,

which also predicts a decrease in the pairing content (pairing correlation energy) with increasing $I$.

Finally, it should be noted that the experimental energies can also be well reproduced under the assumption of a rigid triaxial rotor with $\gamma = 30°$, where $\gamma$ measures the degree of nonaxiality [24]. Recent beyond-mean-field calculations within the generator coordinate method framework [28], which includes triaxial configurations, also show good agreement with the data. However, the SDPF-U-MIX shell-model calculations discussed here clearly predict an axial prolate deformation ($\gamma \sim 0°$). Furthermore, ground-state magnetic moments in the neighboring $^{31}$Mg and $^{33}$Mg are consistent with a prolate axially symmetric rotor coupled to the valence neutron or neutron hole [29,30], while a particle-rotor calculation [31] assuming a triaxially deformed $^{32}$Mg core fails to account for the experimental magnetic moment in $^{31}$Mg.

In summary, the low-energy yrast structure in $^{32}$Mg was populated directly following fragmentation of a secondary $^{46}$Ar beam at the NSCL. This intermediate-energy reaction, involving the removal of 14 nucleons, populates higher angular-momentum states. A new state at 4097(7) keV has been assigned to be the $6^+$ member of the ground-state rotational band in $^{32}$Mg, based on observed $\gamma$-$\gamma$ coincidence, the relative population of states, and comparison to shell-model calculations. The ground-state band in $^{32}$Mg, in particular the observed change in moment of inertia between the ground state and $6^+$ state, is well reproduced by large-scale shell-model calculations using the state-of-the-art SDPF-U-MIX effective interaction, which provide a microscopic interpretation centered on substantial mixing between the 2p-2h and 4p-4h "pure" bands. A mean-field-based (cranked shell model) analysis of the spectrum of rotational states provides intriguing evidence for a reduction in pairing correlations with increased angular momentum. This is consistent with the shell-model results which also show an overall decrease in the pairing content of the band with increasing $I$. Further experimental effort is required to identify the next states in the ground-state band if they are bound; with re-accelerated radioactive beams at fragmentation facilities and increasing beam intensities at the isotope separator on-line (ISOL) at GSI facilities, multistep Coulomb excitation may soon be possible and will provide important information in this region.

[1] T. Otsuka *et al.*, Phys. Rev. Lett. **87**, 082502 (2001).
[2] C. Thibault *et al.*, Phys. Rev. C **12**, 644 (1975).
[3] X. Campi, H. Flocard, A. K. Kerman, and S. Koonin, Nucl. Phys. A **251**, 193 (1975).
[4] B. H. Wildenthal, M. S. Curtin, and B. A. Brown, Phys. Rev. C **28**, 1343 (1983).
[5] A. Poves and J. Retamosa, Phys. Lett. B **184**, 311 (1987).
[6] E. K. Warburton, J. A. Becker, and B. A. Brown, Phys. Rev. C **41**, 1147 (1990).
[7] O. Sorlin and M. Porquet, Prog. Part. Nucl. Phys. **61**, 602 (2008).
[8] K. Wimmer *et al.*, Phys. Rev. Lett. **105**, 252501 (2010).
[9] S. Paschalis *et al.*, Nucl. Instrum. Methods Phys. Res., Sect. A **709**, 44 (2013).
[10] M. de Jong, A. V. Ignatyuk, and K.-H. Schmidt, Nucl. Phys. A **613**, 435 (1997).
[11] D. Morrissey, B. Sherrill, M. Steiner, A. Stolz, and I. Wiedenhoever, Nucl. Instrum. Methods Phys. Res., Sect. B **204**, 90 (2003).
[12] D. Bazin, J. Caggiano, B. Sherrill, J. Yurkon, and A. Zeller, Nucl. Instrum. Methods Phys. Res., Sect. B **204**, 629 (2003).
[13] D. C. Radford, Nucl. Instrum. Methods Phys. Res., Sect. A **361**, 306 (1995).
[14] S. Takeuchi *et al.*, Phys. Rev. C **79**, 054319 (2009).
[15] V. Tripathi *et al.*, Phys. Rev. C **77**, 034310 (2008).
[16] T. Motobayashi *et al.*, Phys. Lett. B **346**, 9 (1995).
[17] B. V. Pritychenko *et al.*, Phys. Lett. B **461**, 322 (1999).
[18] V. Chiste *et al.*, Phys. Lett. B **514**, 233 (2001).
[19] J. A. Church *et al.*, Phys. Rev. C **72**, 054320 (2005).
[20] A. Obertelli *et al.*, Phys. Rev. C **73**, 044605 (2006).
[21] G. Klotz *et al.*, Phys. Rev. C **47**, 2502 (1993).
[22] C. M. Mattoon *et al.*, Phys. Rev. C **75**, 017302 (2007).
[23] E. Caurier, F. Nowacki, and A. Poves, Phys. Rev. C **90**, 014302 (2014), and references therein.
[24] A. Bohr and B. R. Mottelson, *Nuclear Structure* (W. A. Benjamin, Inc., Advanced Book Program, Reading, 1975), Vol. II.
[25] R. Bengtsson and S. Frauendorf, Nucl. Phys. A **327**, 139 (1979).
[26] R. Bengtsson, S. Frauendorf, and F. R. May, At. Data Nucl. Data Tables **35**, 15 (1986).
[27] S. Frauendorf, Nucl. Phys. A **677**, 115 (2000).
[28] M. Borrajo, T. R. Rodriguez and J. Luis Egido, Phys. Lett. B **746**, 341 (2015).
[29] M. Kowalska *et al.*, Phys. Rev. C **77**, 034307 (2008).
[30] D. T. Yordanov *et al.*, Phys. Rev. Lett. **99**, 212501 (2007).
[31] S. E. Larsson, G. Leander, and I. Ragnarsson, Nucl. Phys. A **307**, 189 (1978).